Evaluation of the $\gamma n \to \pi^- p$ differential cross section in the Δ-isobar region

W. J. Briscoe,[1] A. E. Kudryavtsev,[2,1] P. Pedroni,[3] I. I. Strakovsky,[1] V. E. Tarasov,[2] and R. L. Workman[1]
[1]*The George Washington University, Washington, DC 20052, USA*
[2]*Institute of Theoretical and Experimental Physics, Moscow, 117259, Russia*
[3]*INFN, Sezione di Pavia, via Bassi 6, 27100 Pavia, Italy*
(Received 16 October 2012; published 20 December 2012)

Differential cross sections for the process $\gamma n \to \pi^- p$ have been extracted from MAMI-B measurements of $\gamma d \to \pi^- pp$, accounting for final-state interaction effects, using a diagrammatic technique taking into account the NN and πN final-state interaction amplitudes. Results are compared to previous measurements of the inverse process, $\pi^- p \to n\gamma$, and recent multipole analyses.

DOI: 10.1103/PhysRevC.86.065207 PACS number(s): 14.20.Gk, 13.60.Le, 25.10.+s, 25.20.−x

I. INTRODUCTION

An accurate evaluation of the electromagnetic (EM) couplings $N^*(\Delta^*) \to \gamma N$ from meson photoproduction data remains a paramount task in hadron physics. A wealth of new data for meson photoproduction is becoming available from nuclear facilities worldwide. These measurements are now beginning to have a significant impact on both the resonance spectrum and its decay properties.

Here we focus on the single-pion production data and note that a complete solution requires couplings from both charged and neutral resonances, the latter requiring $\pi^- p$ and $\pi^0 n$ photoproduction off a neutron target, typically a neutron bound in a deuteron target. Extraction of the two-body ($\gamma n \to \pi^- p$ and $\gamma n \to \pi^0 n$) cross sections requires the use of a model-dependent nuclear correction, which mainly comes from final-state interactions (FSI). As a result, our knowledge of the neutral resonance couplings is less precise as compared to the charged values [1].

In addition to being less precise, experimental data for neutron-target photoreactions are much less abundant than those utilizing a proton target, constituting only about 15% of the present SAID database [2]. At low to intermediate energies, this lack of neutron-target data is partially compensated by experiments using pionic beams, e.g., $\pi^- p \to \gamma n$, as has been measured, for example, by the Crystal Ball Collaboration at BNL [3] for the inverse photon energy $E_\gamma = 285$–689 MeV and $\theta = 41^\circ$–148°, where θ is the inverse production angle of π^- in the center-of-mass (CM) frame. This process is free from complications associated with the deuteron target. However, the disadvantage of using the reaction $\pi^- p \to \gamma n$ is the 5 to 500 times larger cross sections for $\pi^- p \to \pi^0 n \to \gamma\gamma n$, depending on E_γ and θ.

We recently applied our FSI corrections [4] to CLAS $\gamma d \to \pi^- pp$ data [5] to get elementary cross sections for $\gamma n \to \pi^- p$ [6]. The FSI correction factor for the CLAS kinematics was found to be small, $\Delta\sigma/\sigma < 10\%$. However, these new cross sections departed significantly from our predictions, at the higher energies, and greatly modified the fit result.

The present paper is addressed to differential cross section measurements for $\gamma n \to \pi^- p$ in the $\Delta(1232)$-isobar region. At energies dominated by the Delta resonance, the isospin 3/2 multipoles are constrained by extensive studies performed using proton targets. The forward-peaking structure is due largely to the Born contribution, which is well known. As a result, one would expect models to give predictions within a tight range, which is confirmed in Figs. 1 and 5.

The paper is organized as follows. In Sec. II, we present the new data set and compare it with previous data from hadronic facilities. Section III is devoted to the nuclear corrections. Here, we give comments on the bound neutron and discuss the effect of FSI corrections. In Sec. IV, we correct the new data for FSI and compare them with previous hadronic data and with predictions based on previous multipole analyses. The results of a fit are presented and considered along with the prospect of future polarized measurements.

II. DATA SET

In 2010, the GDH and A2 Collaborations published [7,8] the first measurement of the unpolarized and the helicity-dependent differential cross section for the $\gamma d \to \pi^- pp$ reaction in the Δ-resonance region.

The events from this reaction were selected by requiring the presence of one charged pion and of one or two protons within the detector acceptance (with the momentum threshold for protons and charged pions being $\sim$270 and $\sim$80 MeV/c, respectively, and with full azimuthal acceptance and polar laboratory angular acceptance of between 21° and 159°)

The obtained results consist of 126 experimental points covering an E_γ range from 301 to 455 MeV and a pion polar angular emission range in the CM system between $\theta = 58^\circ$ and $\theta = 141^\circ$.

During the data analysis phase, a kinematic calculation was performed to evaluate the momentum and the emission angle of the undetected proton. The calculated momentum distribution was found to be almost equal to the Fermi momentum distribution expected from the deuteron wave function (see Fig. 1 of Ref. [7]).

This comparison indicates that the dominant mechanism of the $\gamma d \to \pi^- pp$ channel is the quasi-free reaction on the bound neutron while the proton acts merely as a spectator, remaining approximately at rest in the laboratory system.

MAMI-B deuteron data give only the differential cross section as a function of the pion production laboratory angle, and full kinematics was not restored. Thus, the $\gamma n \to \pi^- p$ cross section was extracted by assuming the neutron to be

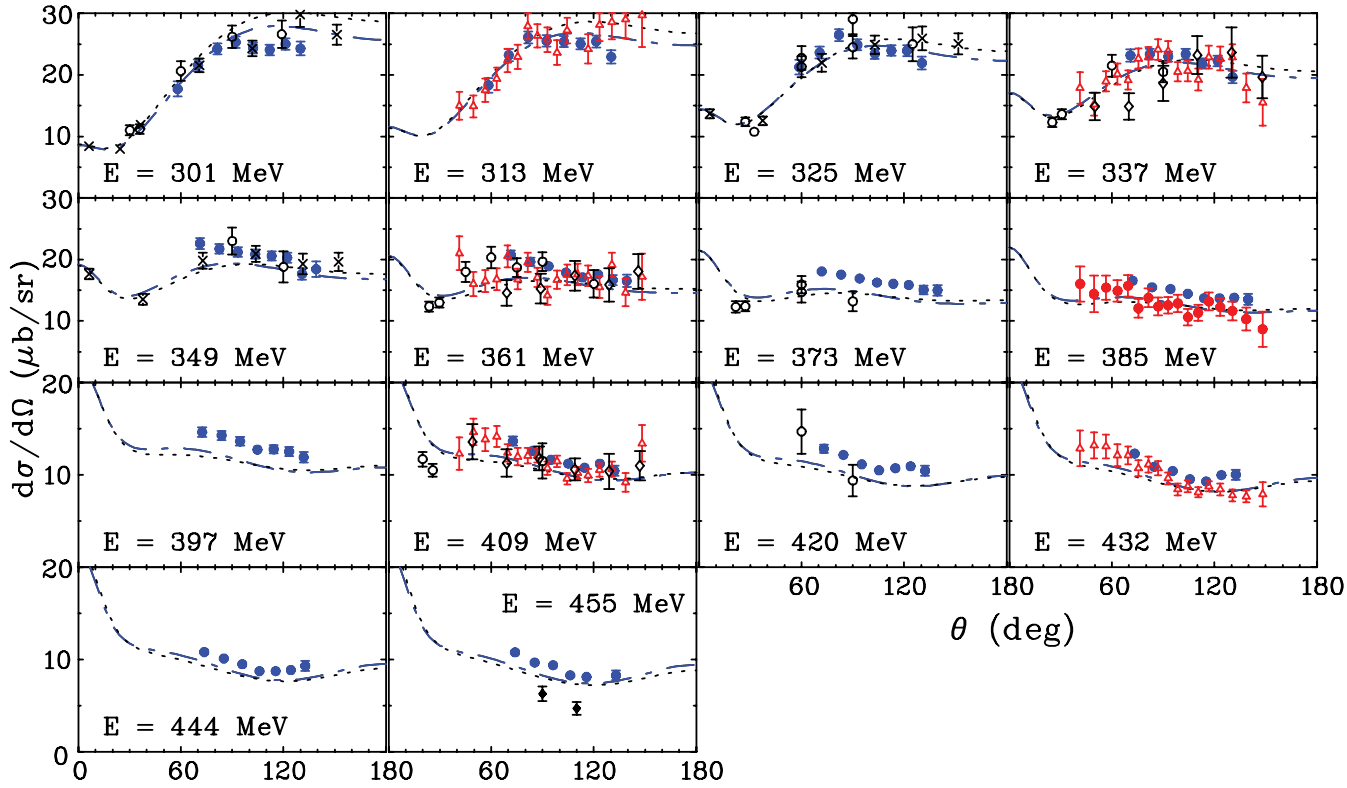

FIG. 1. (Color online) Differential cross sections for $\gamma n \to \pi^- p$ as a function of θ, the production angle of π^- in the CM frame. The present data (solid circles) are shown for 14 energy bins. Previous data came from MAMI-B [7] (blue filled circles), TRIUMF [9] [296, 321, and 346 MeV (black crosses)] CERN [10] [301, 321, 339, 344, 356, 376, 411, and 418 (black open circles)], BNL [3] [313, 338, 359, 390, 407, and 436 MeV (red open triangles)], LBL [11] [335, 355, 360, and 409 MeV (black open diamonds)], and LAMPF [12] [458 MeV (black filled diamonds)]. The data shown came from hadronic facilities, except for MAMI-B measurements (within $\Delta E_\gamma = 5$ MeV binning). Plotted uncertainties are statistical only. Blue dash-dotted (black dotted) lines correspond to the predictions for our recent SN11 [13] (MAID07 [14]) solution.

at rest to unambiguously relate the pion production angles θ in the $\pi^- p$ CM rest frame to their measured laboratory angles.

Specific examples of agreement with previous measurements are displayed in Fig. 1, where we compare differential cross sections obtained here with those from hadronic facilities (TRIUMF [9], CERN [10], BNL [3], LBL [11], and LAMPF [12]), at energies common to those experiments (within $\Delta E_\gamma = 5$ MeV binning).

III. FSI CALCULATIONS

We extract the $\gamma n \to \pi^- p$ cross section on a free nucleon from the deuteron data in the quasi-free (QF) kinematical region of the $\gamma d \to \pi^- pp$ reaction with fast knocked-out proton and slow proton-spectator assumed not to be involved in the pion production process. In this, so-called impulse approximation (IA), the reaction mechanism corresponds to the diagram in Fig. 2(a), and the differential cross section on the deuteron can be related to that on the neutron target in the well-known way (e.g., Eq. (22) of Ref. [4] and references therein). This approximation, with the additional assumption that the neutron is at rest in the deuteron, allows us to identify the cross section $\frac{d\sigma}{d\Omega}$ on the deuteron with that on the neutron, where Ω is the solid angle of the outgoing pion in the γn rest frame. Finally, we use the relation

$$\frac{d\sigma}{d\Omega}(\gamma n) = R^{-1} \frac{d\sigma}{d\Omega}(\gamma d), \tag{1}$$

where R is the FSI correction factor, which takes into account the FSI effects discussed below as well as the identity of two protons in the γd reaction. The right-hand side of Eq. (1) contains the cross sections, $\frac{d\sigma}{d\Omega}(\gamma d)$, in the γn rest frame. They were obtained by recalculation of the data [8] on the cross sections, $\frac{d\sigma}{d\Omega}(\gamma d)$, given in the laboratory system (see Tables I and II), by assuming the neutron to be at rest.

There are two critical factors to be discussed when using this approach: 1. the neutron is bound and 2. there are NN-FSI and πN-FSI effects.

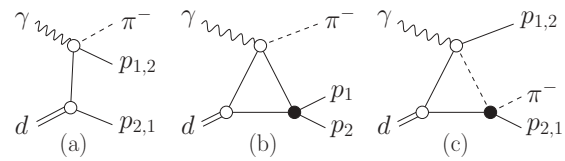

FIG. 2. Feynman diagrams for the leading terms of the $\gamma d \to \pi^- pp$ amplitude. (a) IA, (b) pp-FSI, and (c) πN-FSI. Filled black circles show FSI vertices. Wavy, dashed, solid, and double lines correspond to photons, pions, nucleons, and deuterons, respectively.

TABLE I. Differential cross sections for $\gamma d \to \pi^- pp$ [8] (with statistical and systematical uncertainties given separately, which we then combined in quadrature) and final $\gamma n \to \pi^- p$ below 400 MeV. The differential cross section, $\frac{d\sigma}{d\Omega}(\gamma d)$, is given in the laboratory frame while $\frac{d\sigma}{d\Omega}(\gamma n)$ is given in the CM frame.

Energy (MeV)	$\theta_{\rm lab}$ (deg)	$\frac{d\sigma}{d\Omega}(\gamma d)$ (μb/sr)	θ (deg)	$\frac{d\sigma}{d\Omega}(\gamma n)$ (μb/sr)	Energy (MeV)	$\theta_{\rm lab}$ (deg)	$\frac{d\sigma}{d\Omega}(\gamma d)$ (μb/sr)	θ (deg)	$\frac{d\sigma}{d\Omega}(\gamma n)$ (μb/sr)
301.0	45.0	$18.73 \pm 1.09 \pm 0.68$	58.1	17.71 ± 1.22	313.0	45.0	$20.38 \pm 1.08 \pm 0.74$	58.4	18.30 ± 1.18
	55.0	$23.70 \pm 0.74 \pm 0.76$	70.0	21.59 ± 0.97		55.0	$26.54 \pm 0.71 \pm 0.85$	70.3	23.22 ± 0.97
	65.0	$25.96 \pm 0.54 \pm 0.83$	81.3	24.23 ± 0.93		65.0	$28.49 \pm 0.53 \pm 0.91$	81.6	26.11 ± 0.97
	75.0	$25.20 \pm 0.43 \pm 0.81$	92.1	25.30 ± 0.92		75.0	$25.68 \pm 0.42 \pm 0.82$	92.3	25.52 ± 0.92
	85.0	$22.28 \pm 0.38 \pm 0.69$	102.3	24.37 ± 0.86		85.0	$23.33 \pm 0.39 \pm 0.72$	102.6	25.39 ± 0.89
	95.0	$20.11 \pm 0.38 \pm 0.62$	112.0	24.06 ± 0.87		95.0	$20.95 \pm 0.38 \pm 0.65$	112.3	25.05 ± 0.90
	105.0	$19.13 \pm 0.42 \pm 0.59$	121.2	25.02 ± 0.95		105.0	$19.38 \pm 0.42 \pm 0.60$	121.4	25.44 ± 0.96
	115.0	$17.05 \pm 0.47 \pm 0.62$	130.0	24.28 ± 1.11		115.0	$15.98 \pm 0.47 \pm 0.58$	130.2	22.92 ± 1.07
	125.0	$14.47 \pm 0.59 \pm 0.53$	138.3	22.28 ± 1.22		125.0	$14.36 \pm 0.63 \pm 0.52$	138.5	22.34 ± 1.27
325.0	45.0	$24.88 \pm 1.04 \pm 0.91$	58.7	21.27 ± 1.18	337.0	45.0	$26.35 \pm 1.28 \pm 0.96$	58.9	21.60 ± 1.31
	55.0	$27.84 \pm 0.66 \pm 0.89$	70.5	23.62 ± 0.94		55.0	$27.93 \pm 0.80 \pm 0.89$	70.9	23.17 ± 1.00
	65.0	$29.33 \pm 0.50 \pm 0.94$	81.9	26.48 ± 0.96		65.0	$26.23 \pm 0.46 \pm 0.84$	82.2	23.39 ± 0.85
	75.0	$25.25 \pm 0.41 \pm 0.81$	92.7	24.88 ± 0.89		75.0	$23.49 \pm 0.39 \pm 0.75$	93.0	22.97 ± 0.83
	85.0	$21.60 \pm 0.37 \pm 0.67$	102.9	23.42 ± 0.83		85.0	$21.62 \pm 0.38 \pm 0.67$	103.2	23.38 ± 0.83
	95.0	$20.00 \pm 0.38 \pm 0.62$	112.5	23.95 ± 0.87		95.0	$18.20 \pm 0.37 \pm 0.56$	112.8	21.83 ± 0.81
	105.0	$18.13 \pm 0.41 \pm 0.56$	121.7	23.93 ± 0.92		105.0	$16.78 \pm 0.41 \pm 0.52$	122.0	22.27 ± 0.88
	115.0	$15.15 \pm 0.47 \pm 0.55$	130.4	21.92 ± 1.05		115.0	$13.47 \pm 0.46 \pm 0.49$	130.6	19.66 ± 0.98
	125.0	$13.36 \pm 0.63 \pm 0.49$	138.7	21.03 ± 1.25		125.0	$12.31 \pm 0.64 \pm 0.45$	138.9	19.59 ± 1.24
349.0	45.0	$26.48 \pm 0.90 \pm 0.96$	59.2	20.99 ± 1.05	361.0	45.0	$26.32 \pm 0.68 \pm 0.96$	59.5	20.32 ± 0.91
	55.0	$27.74 \pm 0.59 \pm 0.89$	71.2	22.60 ± 0.87		55.0	$25.83 \pm 0.44 \pm 0.83$	71.5	20.74 ± 0.75
	65.0	$24.64 \pm 0.44 \pm 0.79$	82.5	21.73 ± 0.80		65.0	$22.48 \pm 0.34 \pm 0.72$	82.8	19.62 ± 0.70
	75.0	$21.82 \pm 0.38 \pm 0.70$	93.3	21.19 ± 0.77		75.0	$19.59 \pm 0.29 \pm 0.63$	93.6	18.90 ± 0.67
	85.0	$19.34 \pm 0.36 \pm 0.60$	103.5	20.86 ± 0.75		85.0	$16.63 \pm 0.27 \pm 0.51$	103.8	17.89 ± 0.62
	95.0	$17.14 \pm 0.36 \pm 0.53$	113.1	20.58 ± 0.77		95.0	$14.22 \pm 0.27 \pm 0.44$	113.4	17.08 ± 0.62
	105.0	$15.22 \pm 0.39 \pm 0.47$	122.2	20.29 ± 0.81		105.0	$13.15 \pm 0.30 \pm 0.41$	122.5	17.59 ± 0.68
	115.0	$12.00 \pm 0.45 \pm 0.44$	130.9	17.65 ± 0.92		115.0	$11.25 \pm 0.36 \pm 0.41$	131.1	16.66 ± 0.81
	125.0	$11.46 \pm 0.65 \pm 0.42$	139.1	18.43 ± 1.24		125.0	$10.18 \pm 0.51 \pm 0.37$	139.3	16.52 ± 1.02
373.0	45.0	$24.47 \pm 0.50 \pm 0.89$	59.8	18.50 ± 0.77	385.0	45.0	$23.06 \pm 0.49 \pm 0.84$	60.1	17.12 ± 0.72
	55.0	$22.77 \pm 0.32 \pm 0.73$	71.8	18.05 ± 0.63		55.0	$21.11 \pm 0.30 \pm 0.68$	72.1	16.55 ± 0.58
	65.0	$20.29 \pm 0.26 \pm 0.65$	83.2	17.54 ± 0.61		65.0	$18.05 \pm 0.24 \pm 0.58$	83.5	15.47 ± 0.54
	75.0	$17.64 \pm 0.23 \pm 0.57$	93.9	16.91 ± 0.59		75.0	$15.94 \pm 0.22 \pm 0.51$	94.3	15.19 ± 0.53
	85.0	$15.16 \pm 0.21 \pm 0.47$	104.1	16.25 ± 0.55		85.0	$13.50 \pm 0.21 \pm 0.42$	104.4	14.43 ± 0.50
	95.0	$13.37 \pm 0.22 \pm 0.41$	113.7	16.05 ± 0.56		95.0	$11.42 \pm 0.20 \pm 0.35$	114.0	13.71 ± 0.49
	105.0	$11.82 \pm 0.24 \pm 0.36$	122.8	15.85 ± 0.59		105.0	$10.18 \pm 0.22 \pm 0.31$	123.0	13.69 ± 0.52
	115.0	$10.12 \pm 0.29 \pm 0.37$	131.4	15.07 ± 0.70		115.0	$9.22 \pm 0.28 \pm 0.34$	131.6	13.80 ± 0.65
	125.0	$9.16 \pm 0.40 \pm 0.33$	139.5	14.98 ± 0.85		125.0	$8.21 \pm 0.44 \pm 0.30$	139.7	13.52 ± 0.88
397.0	45.0	$22.55 \pm 0.42 \pm 0.82$	60.4	16.49 ± 0.67	397.0	55.0	$18.85 \pm 0.28 \pm 0.60$	72.4	14.63 ± 0.52
	65.0	$16.79 \pm 0.24 \pm 0.54$	83.8	14.28 ± 0.50		75.0	$14.39 \pm 0.21 \pm 0.46$	94.6	13.64 ± 0.48
	85.0	$11.95 \pm 0.20 \pm 0.37$	104.7	12.74 ± 0.45		95.0	$10.65 \pm 0.20 \pm 0.33$	114.3	12.78 ± 0.46
	105.0	$9.29 \pm 0.22 \pm 0.29$	123.3	12.53 ± 0.49		115.0	$7.92 \pm 0.27 \pm 0.29$	131.8	11.91 ± 0.59
	125.0	$7.84 \pm 0.42 \pm 0.29$	139.9	13.00 ± 0.84					

Factor 1 means that the effective mass of the neutron

$$m_{\rm eff} = \sqrt{(p_d - p_s)^2} \approx m_n - \epsilon_d - \vec{p}_s^{\,2}/m_N$$

is not equal to the mass of the free neutron, m_n. Here, p_d, p_s, $\vec{p}_s$, ϵ_d, and m_N are the deuteron four-momentum, four- and three-momenta of the spectator, the deuteron binding energy, and the nucleon mass, respectively. Simultaneously, the invariant mass $\sqrt{s_{\pi N}}$ of the final πN system,

$$\sqrt{s_{\pi N}} = \sqrt{s_{\gamma N}} = \sqrt{[(E_\gamma + m_d - E_s)^2 - (\vec{p}_\gamma - \vec{p}_s)^2]},$$

depends on the proton-spectator momentum $\vec{p}_s$ (where $s_{\gamma N}$ is the invariant mass squared of the initial γN state). Here, E_γ (E_s), m_d, and $\vec{p}_\gamma$ are the total energy of the initial photon (proton spectator), the deuteron mass, and the photon three-momentum, respectively, and $E_\gamma = |\vec{p}_\gamma|$.

Since $\sqrt{s_{\pi N}}$ depends on $\vec{p}_s$, the $\gamma N \to \pi N$ cross section extracted from the deuteron data with undetected nucleon spectator is averaged over the energy range, which depends on kinematical cuts for $\vec{p}_s$. Thus, the "effective" photon laboratory energy $E_{\gamma n}$, defined through the relation $s_{\gamma N} = m_n^2 + 2m_n E_{\gamma n}$ for the $\gamma n \to \pi^- p$ reaction, is smeared as well as the pion CM angle θ due the deuteron wave function. We estimated this

TABLE II. Differential cross sections for $\gamma d \to \pi^- pp$ [8] (with statistical and systematical uncertainties given separately, which we then combined in quadrature) and final $\gamma n \to \pi^- p$ above 400 MeV. The differential cross section, $\frac{d\sigma}{d\Omega}(\gamma d)$, is given in the laboratory frame while $\frac{d\sigma}{d\Omega}(\gamma n)$ is given in the CM frame.

Energy (MeV)	$\theta_{\rm lab}$ (deg)	$\frac{d\sigma}{d\Omega}(\gamma d)$ (μb/sr)	θ (deg)	$\frac{d\sigma}{d\Omega}(\gamma n)$ (μb/sr)	Energy (MeV)	$\theta_{\rm lab}$ (deg)	$\frac{d\sigma}{d\Omega}(\gamma d)$ (μb/sr)	θ (deg)	$\frac{d\sigma}{d\Omega}(\gamma n)$ (μb/sr)
409.0	45.0	$21.34 \pm 0.44 \pm 0.78$	60.6	15.40 ± 0.64	420.0	45.0	$20.43 \pm 0.37 \pm 0.74$	60.9	14.58 ± 0.59
	55.0	$17.77 \pm 0.27 \pm 0.57$	72.7	13.66 ± 0.48		55.0	$16.83 \pm 0.27 \pm 0.54$	73.0	12.83 ± 0.46
	65.0	$14.92 \pm 0.23 \pm 0.48$	84.2	12.60 ± 0.45		65.0	$14.48 \pm 0.23 \pm 0.46$	84.5	12.16 ± 0.44
	75.0	$12.32 \pm 0.20 \pm 0.39$	94.9	11.63 ± 0.42		75.0	$11.84 \pm 0.20 \pm 0.38$	95.2	11.14 ± 0.40
	85.0	$10.55 \pm 0.19 \pm 0.33$	105.1	11.22 ± 0.40		85.0	$9.88 \pm 0.19 \pm 0.31$	105.3	10.50 ± 0.38
	95.0	$8.97 \pm 0.19 \pm 0.28$	114.6	10.77 ± 0.40		95.0	$8.91 \pm 0.19 \pm 0.28$	114.9	10.72 ± 0.40
	105.0	$8.28 \pm 0.21 \pm 0.26$	123.6	11.20 ± 0.45		105.0	$8.05 \pm 0.22 \pm 0.25$	123.8	10.93 ± 0.45
	115.0	$6.96 \pm 0.26 \pm 0.25$	132.1	10.43 ± 0.54		115.0	$6.94 \pm 0.27 \pm 0.25$	132.3	10.45 ± 0.56
	125.0	$7.72 \pm 0.48 \pm 0.28$	140.2	12.77 ± 0.92		125.0	$6.92 \pm 0.48 \pm 0.25$	140.3	11.51 ± 0.90
432.0	45.0	$19.41 \pm 0.39 \pm 0.71$	61.2	14.22 ± 0.59	444.0	45.0	$17.83 \pm 0.37 \pm 0.65$	61.5	12.44 ± 0.52
	55.0	$15.89 \pm 0.26 \pm 0.51$	73.3	12.30 ± 0.44		55.0	$14.41 \pm 0.25 \pm 0.46$	73.6	10.80 ± 0.39
	65.0	$12.81 \pm 0.22 \pm 0.41$	84.8	10.87 ± 0.40		65.0	$12.16 \pm 0.22 \pm 0.39$	85.1	10.12 ± 0.37
	75.0	$11.00 \pm 0.20 \pm 0.35$	95.6	10.41 ± 0.38		75.0	$10.14 \pm 0.19 \pm 0.33$	95.9	9.49 ± 0.35
	85.0	$8.94 \pm 0.19 \pm 0.28$	105.7	9.53 ± 0.36		85.0	$8.21 \pm 0.18 \pm 0.25$	106.0	8.74 ± 0.33
	95.0	$7.73 \pm 0.19 \pm 0.24$	115.2	9.29 ± 0.37		95.0	$7.21 \pm 0.18 \pm 0.22$	115.4	8.74 ± 0.35
	105.0	$7.37 \pm 0.22 \pm 0.23$	124.1	9.98 ± 0.43		105.0	$6.45 \pm 0.21 \pm 0.20$	124.4	8.86 ± 0.40
	115.0	$6.61 \pm 0.28 \pm 0.24$	132.5	10.01 ± 0.56		115.0	$6.04 \pm 0.27 \pm 0.22$	132.8	9.31 ± 0.54
	125.0	$7.25 \pm 0.51 \pm 0.26$	140.5	12.15 ± 0.96		125.0	$6.24 \pm 0.50 \pm 0.23$	140.8	10.68 ± 0.94
455.0	45.0	$17.45 \pm 0.37 \pm 0.64$	61.7	12.05 ± 0.51	455.0	55.0	$14.48 \pm 0.26 \pm 0.46$	73.9	10.78 ± 0.40
	65.0	$11.68 \pm 0.22 \pm 0.37$	85.4	9.67 ± 0.36		75.0	$10.03 \pm 0.20 \pm 0.32$	96.2	9.38 ± 0.35
	85.0	$7.76 \pm 0.18 \pm 0.24$	106.3	8.28 ± 0.32		95.0	$6.66 \pm 0.18 \pm 0.21$	115.7	8.11 ± 0.33
	105.0	$7.00 \pm 0.22 \pm 0.22$	124.6	9.67 ± 0.43		115.0	$5.33 \pm 0.28 \pm 0.19$	133.0	8.28 ± 0.53
	125.0	$5.46 \pm 0.51 \pm 0.20$	140.9	9.42 ± 0.95					

smearing from simplified calculation, where the $\gamma d \to \pi^- pp$ amplitude is proportional to the deuteron wave function and depends only on the laboratory momentum of one of the final protons, say p_2, while $E_{\gamma n}$ is determined through the above-mentioned relation with the effective mass of the pion-proton pair with another proton p_1.

Figure 3 shows distributions on $\Delta E = E_{\gamma n} - E_\gamma$ at $E_\gamma =$ 301 and 455 MeV. The distributions peak at $\Delta \approx -3$ MeV, where $E_{\gamma n}$ is very close to E_γ. The dispersion $\sigma(\Delta) =$ 20.3 (32.2) MeV at $E_\gamma = 301$ (455) MeV essentially exceeds

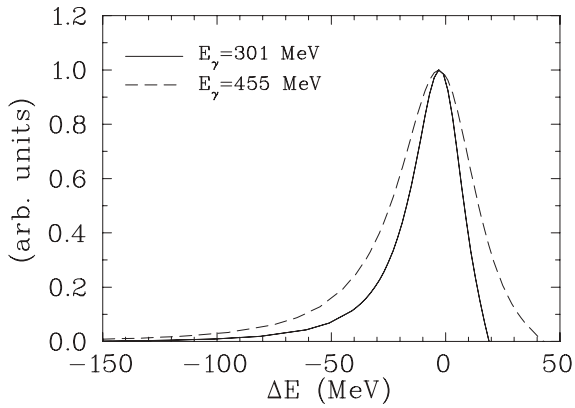

FIG. 3. Distributions on the shift $\Delta E = E_{\gamma n} - E_\gamma$ of the effective photon laboratory energy $E_{\gamma n}$ on the neutron target at $E_\gamma =$ 301 MeV (solid curve) and 455 MeV (dashed curve). The mean values are $\sigma(\Delta) = -12\,(-14.6)$ MeV for $E_\gamma = 301\,(455)$ MeV.

the 12-MeV intervals between the plots on Fig. 1. Thus, the neighbor plots on Fig. 1 are quite similar already due to smearing. The plots on Fig. 1 also weakly depend on the energy E_γ in the intervals $\sim\sigma(\Delta)$. Thus, the distortion of the extracted $\gamma n \to \pi^- p$ cross sections due to the smearing effect is expected to be small.

The results for the pion CM angle smearing in the angular range of MAMI-B data give mean values $\langle\theta\rangle$ very close to θ, namely, $|\langle\theta\rangle - \theta| < 1^\circ$, where the pion CM angles θ are obtained from $\theta_{\rm lab}$ with the neutron at rest. The angle dispersion $\sigma(\theta)$ varies in the interval $\sim$3.0°–5.5°.

Factor 2 corresponds to the inclusion of the FSI corrections. Their leading terms correspond to the Feynman diagrams shown in Figs. 2(b) and 2(c).

Calculations of the $\gamma d \to \pi^- pp$ differential cross sections, with the FSI taken into account (including all the diagrams in Fig. 2), were done as we did recently [4,6] for the CLAS data ($E_\gamma = 1050$–2700 MeV and $\theta = 32^\circ$–157°) [5]. The SAID phenomenological amplitudes for $\gamma N \to \pi N$ [15], $NN \to NN$ [16], and $\pi N \to \pi N$ [17] were used as inputs to calculate the diagrams in Fig. 2. The Bonn potential [18] was used for the deuteron description. In Ref. [6], we calculated the FSI correction factor R dependent on E_γ and θ (see details in Refs. [4,6]) and fitted these CLAS data versus the world $\gamma N \to \pi N$ database [2] to get new multipoles and determine resonance EM couplings [6]. The FSI corrections for the CLAS QF kinematics were found to be small, as mentioned above. Our FSI calculations were done [4] over a broad energy range (threshold to 2700 MeV for E_γ) and for

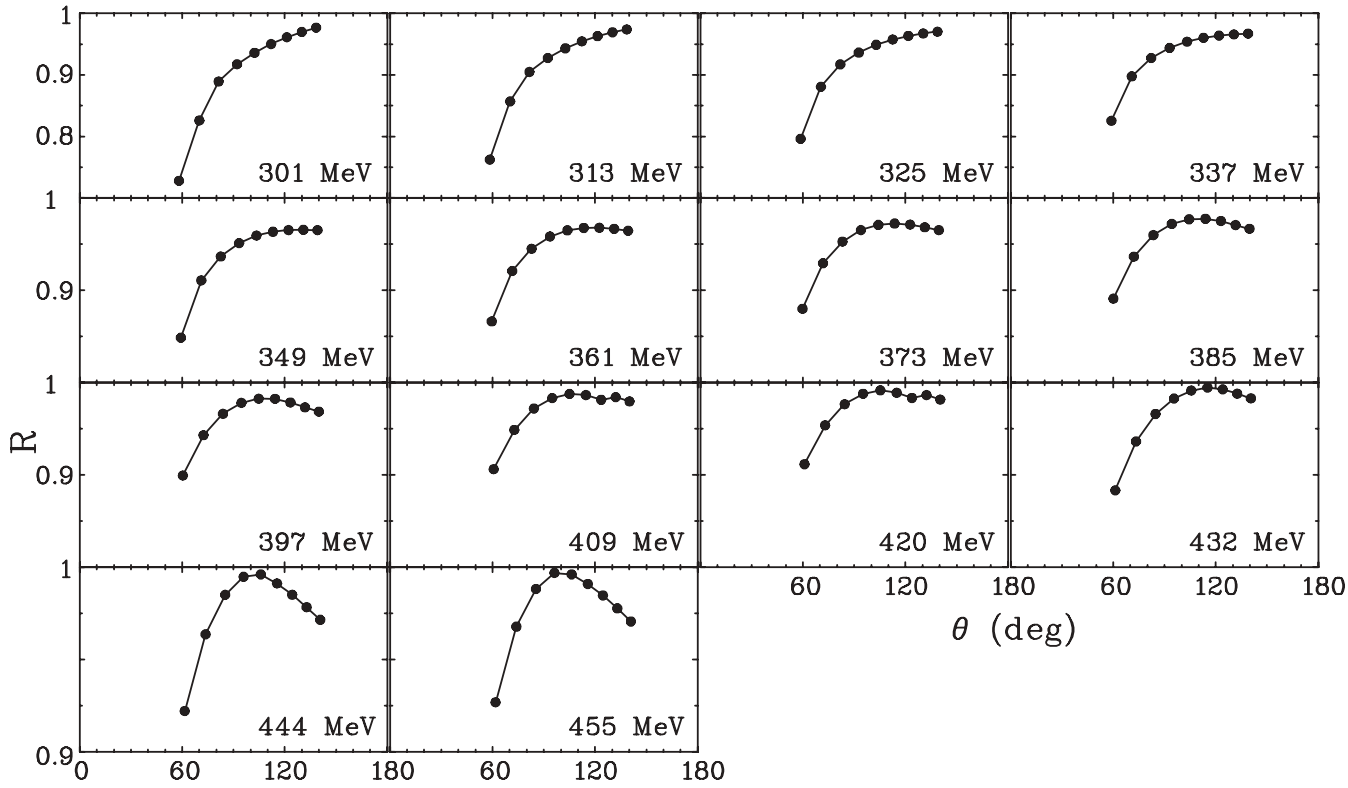

FIG. 4. FSI correction factor R for $\gamma n \to \pi^- p$ as a function of θ, where θ is the production angle of π^- in the CM frame. The present calculations (solid circles) are shown for 14 energy bins. There are no uncertainties given. Curves may help to lead the eyes.

the full angular coverage ($\theta = 0^\circ$–180°). As an illustration, Fig. 4 shows the FSI correction factor $R = R(E_\gamma, \theta)$ for the present $\gamma n \to \pi^- p$ differential cross sections as a function of the pion production angle in the CM($\pi^- p$) frame, θ, for different energies over the range of the MAMI-B experiment. Overall, the FSI correction factor $R < 1$, while the effect, i.e., the $(1 - R)$ value, varied from 10% to 30% depending on the kinematics, and the behavior is very smooth versus pion production angle. Note that $R(E_\gamma, \theta)$ is the FSI correction factor for the $\gamma n \to \pi^- p$ cross section averaged over the laboratory photon energy $E_{\gamma n}$. Figure 2 shows that R depends slowly on the energy in the intervals $\sim\sigma(\Delta)$. Thus, the smearing effect illustrated in Fig. 3 weakly affects the FSI correction procedure for the extracted $\gamma n \to \pi^- p$ cross section at a given energies.

The contribution of FSI calculations [4] to the overall systematics is estimated to be 2%.

IV. RESULTS

In fitting the database, χ^2 is calculated by using

$$\chi^2 = \sum_i^{N_{\rm data}} \left(\frac{O_i - N_j O_i^{\rm exp}}{\delta O_i} \right)^2 + \sum_j^{N_{\rm dist}} \left(\frac{N_j - 1}{\delta N_j} \right)^2, \qquad (2)$$

where O_i and $O_i^{\rm exp}$ are calculated and experimental observables, for a given energy and angle, and δO_i is the statistical uncertainty. The systematic error, δN_j, for a given angular distribution, is used to calculate a second contribution to χ^2 due to overall normalization (N_j) of angular data sets.

In Fig. 1, which compares the present measurements with corresponding results derived from pion-induced reactions, no FSI (nor any data renormalization) corrections have been applied. The curves are predictions from SAID and MAID and are generally quite consistent. Without corrections, the pion- and photo-induced data are reasonably consistent where they can be compared (the pion-induced results having significantly larger uncertainties). Comparisons with the SAID and MAID predictions show reasonable agreement in terms of shape but, at a number of energies, there is a clear difference in the overall normalization.

In Fig. 5, both FSI and data renormalization have been applied. A solid curve, giving the result of a fit, is compared with the aforementioned predictions. The data renormalization, required for a best-fit result, changes from an average of 7%, for the SAID prediction, to about 4.5%, after the data have been included in the fit. In both cases, the second term in Eq. (2) above (due to renormalization) contributes nearly 50% to the total chi-squared value.

Changes to the multipoles in the revised fit are small. The dominant multipole contribution from the $\Delta(1232)$ is not changed significantly, as one would expect. Together with the measurements of Ref. [6], we now have nearly complete coverage of the resonance region for unpolarized cross sections in this reaction. Further progress will require polarized measurements, which are expected from the CLAS Collaboration [19].

The MAMI-B results for the $\gamma d \to \pi^- pp$ differential cross sections in the laboratory frame, $\frac{d\sigma}{d\Omega}(\gamma d)$, consist of 126 experimental points ($E_\gamma = 301$–455 MeV and

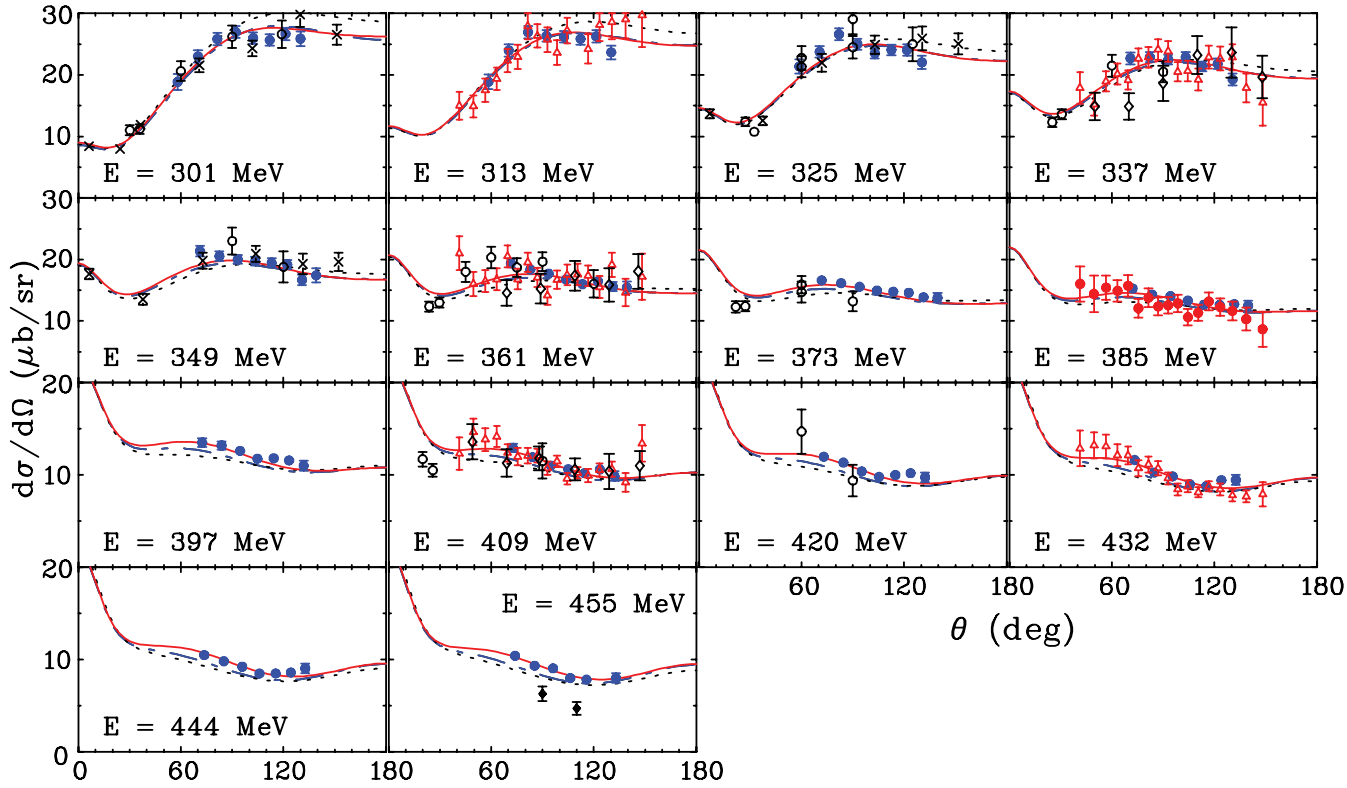

FIG. 5. (Color online) Differential cross sections for $\gamma n \to \pi^- p$ as a function of θ, where θ is the production angle of π^- in the CM frame. Notation of data and solutions are the same as in Fig. 1. MAMI-B data including in the PE12 fit (red solid line).

$\theta_{\rm lab} = 45^\circ$–$125^\circ$); these are tabulated in Ref. [8]. For the reader's convenience these data with the final $\gamma n \to \pi^- p$ ones in the CM frame, $\frac{d\sigma}{d\Omega}(\gamma n)$, are also shown in Tables I and II along with their uncertainties.

The χ^2 contribution of MAMI-B data (including FSI corrections) is $\chi^2/\text{data} = 249.4/104 = 2.4$ while, prior to fitting, for SN11 [13] (MAID07 [14]), we had $\chi^2/\text{data} = 605.8/104 = 5.8$ ($623.2/104 = 6.0$).

The MAMI-B data (including FSI corrections) and the results from hadronic data appear to agree well at these energies (Fig. 4). In particular, the χ^2 contributions from recent Crystal Ball at BNL [3] and MAMI-B measurements at six overlapped energies [313, 337, 361, 385, 409, and 432 MeV] are $\chi^2/\text{data} = 97.7/102 = 1.0$ and $\chi^2/\text{data} = 103.9/45 = 2.3$, respectively, for the PE12 solution, while for the previous SN11 solution [13], $\chi^2/\text{data} = 87.4/102 = 0.9$ and $\chi^2/\text{data} = 188.6/45 = 4.2$, respectively. (MAMI-B data had no FSI corrections.)

V. SUMMARY AND CONCLUSION

A comprehensive set of differential cross sections at 14 energies for negative-pion photoproduction on the neutron, via the reaction $\gamma d \to \pi^- pp$, has been determined with a MAMI-B tagged-photon beam for incident photon energies from 301 to 455 MeV. To accomplish a state-of-the-art analysis, we included FSI corrections using a diagrammatic technique, taking into account a kinematical cut with momenta less (more) than $\sim$270 MeV/c for slow (fast) outgoing protons.

On the experimental side, further improvements in the partial wave analyses await more data, specifically in the region above 1 GeV, where the number of measurements for this reaction is small. Of particular importance in all energy regions is the need for data obtained involving polarized photons and/or polarized targets. Some of these data are already available in Ref. [6]. Due to the closing of hadron facilities, new $\pi^- p \to \gamma n$ experiments are not planned and only $\gamma n \to \pi^- p$ measurements are possible at electromagnetic facilities using deuterium targets. Our agreement with existing π^- photoproduction measurements leads us to believe that these photoproduction measurements are reliable despite the necessity of using a deuterium target.

Obviously, any meson photoproduction treatment on the "neutron" target requires a FSI study. Generally, FSI depend on the full set of kinematical variables of the reaction. In our analysis, the FSI correction factor depends on the photon energy and meson production angle and is averaged over the rest of variables in the region of the QF process on the neutron.

ACKNOWLEDGMENTS

We acknowledge the outstanding efforts of the GDH and A2 Collaborations who made the experiment possible. This work was supported in part by the US Department of Energy Grant No. DE–FG02–99ER41110, by the Russian RFBR Grant No. 02–0216465, by the Russian Atomic Energy Corporation "Rosatom" Grant No. NSb–4172.2010.2, and by the Italian Istituto Nazionale di Fisica Nucleare.

[1] J. Beringer *et al.* (Particle Data Group), Phys. Rev. D **86**, 010001 (2012).
[2] W. J. Briscoe, I. I. Strakovsky, and R. L. Workman, Institute of Nuclear Studies of the George Washington University Database; http://gwdac.phys.gwu.edu/analysis/pr_analysis.html.
[3] A. Shafi *et al.* (Crystal Ball Collaboration), Phys. Rev. C **70**, 035204 (2004).
[4] V. E. Tarasov *et al.*, Phys. Ref. C **84**, 035203 (2011).
[5] W. Chen *et al.* (CLAS Collaboration), Phys. Rev. Lett. **103**, 012301 (2009).
[6] W. Chen, H. Gao, W. J. Briscoe, D. Dutta, A. E. Kudryavtsev, M. Mirazita, M. W. Paris, P. Rossi, S. Stepanyan, I. I. Strakovsky, V. E. Tarasov, and R. L. Workman, Phys. Rev. C **86**, 015206 (2012).
[7] J. Ahrens *et al.* (GDH and A2 Collaborations), Eur. Phys. J. A **44**, 189 (2010).
[8] M. M. Fabregate, Ph.D. thesis, Mainz University, 2007.
[9] M. Wang, Ph.D. thesis, University of Kentucky, 1992.
[10] M. T. Tran *et al.*, Nucl. Phys. A **324**, 301 (1979).
[11] J. C. Comiso *et al.*, Phys. Rev. D **12**, 719 (1975).
[12] G. J. Kim, J. Arends, W. J. Briscoe, J. Engelage, B. M. K. Nefkens, M. E. Sadler, and H. J. Ziock, Phys. Rev. D **40**, 244 (1989).
[13] R. L. Workman, W. J. Briscoe, M. W. Paris, and I. I. Strakovsky, Phys. Rev. C **85**, 025201 (2012).
[14] D. Drechsel, S. S. Kamalov, and L. Tiator, Eur. Phys. J. A **34**, 69 (2007); http://www.kph.uni-mainz.de/MAID/.
[15] M. Dugger *et al.* (CLAS Collaboration), Phys. Rev. C **76**, 025211 (2007).
[16] R. A. Arndt *et al.*, Phys. Rev. C **76**, 025209 (2007).
[17] R. A. Arndt, W. J. Briscoe, I. I. Strakovsky, and R. L. Workman, Phys. Rev. C **74**, 045205 (2006).
[18] R. Machleidt *et al.*, Phys. Rep. **140**, 1 (1987).
[19] D. Sokhan, Ph.D. thesis, Edinburgh University, 2009.